 CMC, vol.21, no.2, pp.147-170, 2011

Nano-Array Solid Electrode Design for Photoelectrochemical Solar Cells

W.H. Chen[1] **and C.W. Hong**[1,2]

Abstract: Nanorod/nanowell/nanotube arrays are effective nanotechnologies that can increase the performance of a photo-electrochemical solar cell by increasing the reaction area of the working electrode. However, the confined space due to the nano-arrays also tends to decrease the redox ion diffusivity. This paper describes computer modeling on the ionic diffusion of the active species (I^-/I_3^-) among the nano-arrays of the working electrode material (TiO_2). A three dimensional periodic boundary molecular dynamics simulation technique is employed to simulate the nano-scale transport phenomenon. Performance improvement tendency can be evaluated from the Butler-Volmer equation. Simulation results reveal that the increasing reaction area times the decreasing diffusion coefficient (due to decreasing porosity) can be optimized at an effective porosity around 0.75 using the nanotube array design. With this optimized design, the current density can be improved by 53% and the power density by 66%.

Keywords: Nanotechnology, Photoelectrochemical solar cells, Molecular dynamics, Nanotube array.

1 Introduction

Photo-electrochemical cells are one of the major subjects of interest in the next generation of solar energy conversion [Grätzel (2009); Green, Emery, Hisikawa, and Warta (2009); Deb (2005)]. This is mainly due to low materials cost (except for the optional ruthenium dyes) and simple fabrication processes for all components. The highest photovoltaic efficiency that has been reported up to date is 11.18% [Chen, Wang, Li, Pootrakulchote, Alibabaei, Ngoc-Le, Decoppet, Tsai, Grätzel, Wu, Zakeeruddin, and Grätzel (2009)] and further improvements are possible. The photovoltaic performance of the dye-sensitized solar cell (DSSC) results from the

[1] Department of Power Mechanical Engineering, National Tsing Hua University (NTHU), Hsinchu, Taiwan.
[2] email: cwhong@pme.nthu.edu.tw (Corresponding author)

photo-excitation of the dye molecules and the subsequent injection of electrons into the TiO_2 conduction band. Increasing the reaction area (for adsorption of optional ruthenium dyes or semiconductor quantum dots) through nanorod, nanowell and nanotube technologies in the fabrication of the TiO_2 electrode [Tao, Wu, Xue, Song, Pan, Fang, Fang, and Dai (2010); Jiu, Isoda, Wang, and Adachi (2006); Kang, Choi, Kang, Kim, Kim, Hyeon, and Sung (2008); Lee, Song, Jang, Jo, Kwak, and Kim (2009); Marco, Manca, Giannuzzi, Malara, Melcarne, Ciccarella, Zama, Cingolani, and Gigli (2010); Paula, Colavita, Doescher, Schiza, and Myrick (2002); Ide, Fujimoto, Kado, and Hayase (2008); Roy, Kim, Lee, Spiecker, and Schmuki (2010); Gong, Grimes, Varghese, Hu, Singh, Chen, and Dickey (2001); Kim, Ghicov, Albu, and Schmuki (2008); Kislyuk, and Dimitriev (2008); Xu, Shin, Cao, Wu, and Gai (2010), Li, Saheli, Khaleel, and Garmestani (2006)] is one of the simplest and least cost methods available. Chen, Jehng, Li, and Diau (2009) attained a maximum performance efficiency of 6.18% in their experimental work on nanotubes. The schematic diagram of a novel nano-array DSSC system is shown in Figure 1(a) and three kinds of designs of the nanorod, nanowell, and nanotube arrays in this research are shown in Figure 1(b, c, d), respectively. Using these nanotechnologies to fabricate the porous working electrode, a large surface area for adsorption of a large number of dye molecules to react with the redox electrolyte can be achieved.

The first step of this research is to model the molecular diffusion mechanism and to validate the diffusion coefficient values via simulations and experiments at the same time. However, the effective diffusion coefficient (porosities smaller than 1) values in the nanochannels are too difficult to measure via experiments because of the confined space involved. That limits our experiments to measure the free diffusion coefficient (porosity equal to 1, i.e. in absence of nanostructures). Still, the limited comparison can give an idea of the accuracy of the simulation. If an acceptable accuracy is reached in the molecular free diffusion simulation, the next step is to apply the technique with the nano-array boundaries (with porosities less than 1).

The effective diffusion coefficient in the porous medium times the effective reaction area of the nano-array design is the key parameter that influences the DSSC performance. Each nano-array design yields a different reaction area and effective diffusion coefficients under different porosities. The first two TiO_2 molecular structures to model are the nanorod and nanowell array designs. These two array designs are later combined to form an ordered nanotube design. A periodic boundary molecular dynamics technique [Lee, and Hong (2009); Chen, Chiu, and Hong (2009); Chen, Chen, and Hong (2009)] is used to simulate the nano-array patterns by repeating each unit cell in three dimensions. The dynamic transport phenomenon of each species was observed and the effective transport properties

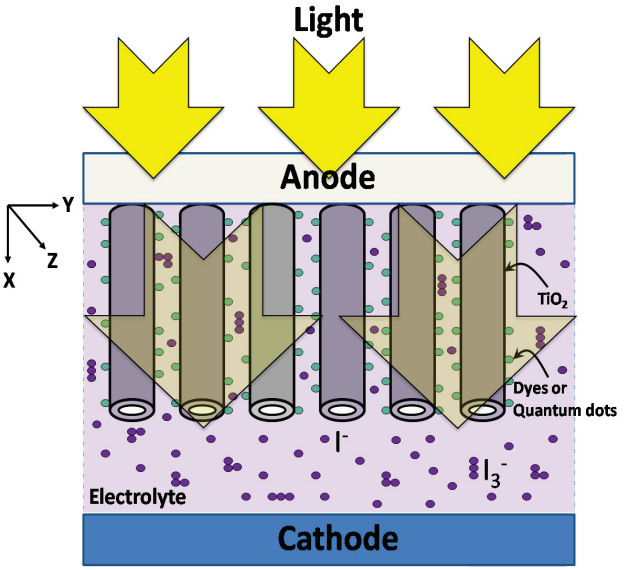

(a)

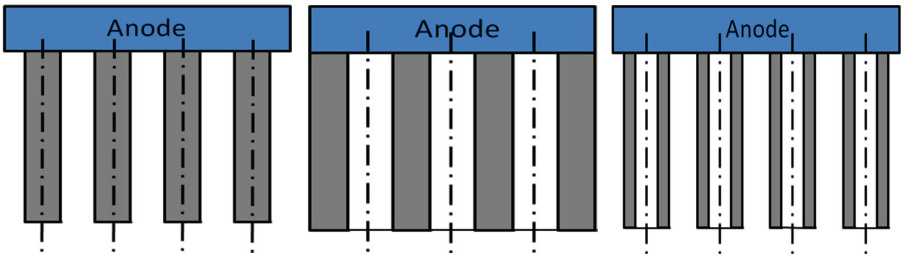

(b) nanorod (c) nanowell (d) nanotube

Figure 1: (a) Schematic diagram of a novel nano-array photoelectrochemical cell with three nano-array designs: (b) nanorod, (c) nanowell, and (d) nanotube

were later assessed through statistical thermodynamics techniques. The ultimate objective is to optimize the nano-array design parameters, such as geometry and dimensions, by comparing their respective molecular simulation results. The following sections describe the fundamental theory of molecular modeling, the free diffusion coefficient experiment and the result analyses with different nano-array designs.

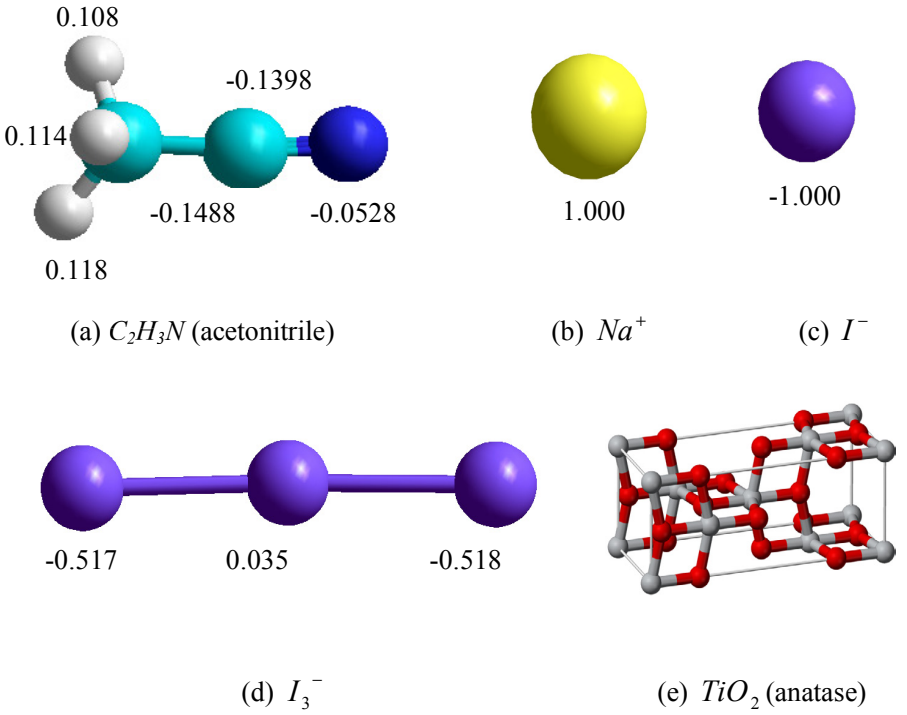

(a) C_2H_3N (acetonitrile) (b) Na^+ (c) I^-

(d) I_3^- (e) TiO_2 (anatase)

Figure 2: Molecular structure and charge distribution of the electrochemical species in the electrolyte: (a) C_2H_3N (acetonitrile), (b) Na^+, (c) I^- , (d) I_3^- , and (e) the working electrode in the form of anatase TiO_2.

2 Molecular Simulation System

The molecular simulation system in this study mainly consists of five molecular species, namely: iodide (I^-), tri-iodide (I_3^-), sodium ions (Na^+), acetonitrile (C_2H_3N) molecules and the working electrode of titanium dioxide (TiO_2). Figures 2(a)-2(d) show the molecular structures and charge distribution of each species in the electrolyte. Figure 2(e) shows the titanium dioxide structure which is mainly in the anatase configuration. The rutile and brookite configurations in the TiO_2 structure are the minority and thus neglected. The initial conformations and charge distributions for each molecule were constructed by a semi-empirical quantum method (Austin model 1) [Hypercube Inc. (2002)]. The calculation was considered to converge when the gradient of the atomic potential was less than the preset value of 0.01 kcal mol^{-1} $Å^{-1}$. Once convergence was attained, an optimal geometry in minimum energy was constructed and the distribution of charges was assigned.

The number of iodide ions is assigned according to the optimized concentration of $0.5M\ I^- + 0.055M\ I_3{}^-$ [Chen, Miranda, and Hong (2011)] and a mass concentration of $0.786g \cdot cm^{-3}$ obtained from a free diffusion experiment. The number of tri-iodide ions was calculated according to the concentration of $0.055M\ I_3{}^-$ with the minimum molecule number greater than or equal to 1. The number of sodium ions equals the number of iodide plus the tri-iodide ions to achieve a neutral solution. Acetonitrile molecules are added into the unit cell to adjust the mass concentration to $0.786g \cdot cm^{-3}$ according to the experimental data described in the next section.

The number of TiO_2 molecules for nanorod and nanotube structures is fixed (constant volume and height) and the system volume is varied to change the equivalent porosity, defined as the ratio of the void volume divided by the system volume (shown in Table 1). To vary the equivalent porosity in the nanowell and nanotube structures, the void space's volume was slightly varied and the number of TiO_2 molecules increased (shown in Table 2 and 3, respectively). The TiO_2 molecules act as solid walls and the other active molecules are free to move and are initially assigned to distribute randomly inside the simulation system, as shown in Figure 3. The unit cell diagrams show that the self-assembled molecular structure of the anatase TiO_2 is more or less an octagon from the top view of the nanorod array, which is similar to photos taken in most experiments [Xu, Shin, Cao, Wu, and Gai (2010); Chen, Jehng, Li, and Diau (2009)]. Figures 4 and 5 show the molecule distribution of each species in the unit cells of the nanowell and nanotube structures.

As mentioned earlier, the nanotube structure is the combination of both nanorod and nanowell structures. The effective porosity of a nanotube array is 10 % greater than the nanorod or nanowell structure, making this hybrid construction the most effective way to increase the reaction area in nano-array designs enabling a potential increase in the system performance.

3 Molecular Dynamics

In the Hamiltonian system, the total energy is expressed by:

$$U_{total} = U_{inter} + U_{intra} + KE \tag{1}$$

where U_{total} is the total energy, U_{inter} is the inter-molecular potential energy, U_{intra} is the intra-molecular potential energy, and KE is the kinetic energy. The inter-molecular potential includes both the van der Waals and electrostatic potentials. The van der Waals force was expressed by a typical 12-6 Lennard-Jones function. The electrostatic potential at the periodic boundary was handled by an Ewald summation method [Allen, and Tildesley (1987)]. For multi-atom molecules, the intra-molecular potential includes the valence angle potential (U_{angle}), the bond potential

Table 1. Summary of the number of molecules of each species in the nanorod structure unit cell with different equivalent porosities but fixed molar concentration of *0.5 MI^-* and fixed mass concentration around *0.786 g.cm^{-3}*

Nanorod structure	Equivalent porosity					
	0.50	0.55	0.60	0.65	0.70	0.75
Void volume (Å^3)	18530	22647	27795	36958	43236	55590
Total system volume (Å^3)	37060	41177	46325	55488	61766	74120
No. of iodide ions	6	7	8	11	13	17
No. of tri-iodide ions	1	1	1	1	1	2
No. of sodium ions	7	8	9	12	14	19
No. of acetonitrile molecules	182	226	281	376	442	560
No. of TiO_2 molecules	532	532	532	532	532	532

$$I^- \text{ concentration} \quad \mathrm{M} = \frac{\text{no. of } I^- \text{ ions}}{\text{void volume} \times 6 \times 10^{23} \times 10^{-27}}$$

$$\text{Equivalent porosity}\,(\%) = \frac{\text{total volume of the void space}}{\text{total system volume}}$$

(U_{bond}), and the dihedral angle potential ($U_{dihedral}$). These potential functions are expressed by:

$$U_{angle}(\theta) = \frac{k_a}{2}(\cos\theta - \cos\theta_0)^2 \tag{2}$$

$$U_{bond}(r_{ij}) = \frac{k_b}{2}(r_{ij} - r_0)^2 \tag{3}$$

$$U_{dihedral}(\phi) = A\,[1 + \cos(m\phi - \delta)] \tag{4}$$

where k_a and k_b are force parameters of the angle and the bond potentials; A, m and δ are parameters in the dihedral potential function; θ and ϕ are the bond and the torsion angles. The aforenamed parameters for the acetonitrile molecules and tri-iodide ions were obtained from the DREIDING force field developed by Mayo, Olfason, and Goddard (1990).

Table 2. Summary of the number of molecules of each species in the unit cells of the nanowell structure with different equivalent porosities

Nanowell structure	Equivalent porosity					
	0.50	0.55	0.60	0.65	0.70	0.75
Void volume ($Å^3$)	11854	14488	17781	22016	27659	35562
Total system volume ($Å^3$)	23708	26342	29635	33870	39513	47416
No. of iodide ions	4	5	6	7	9	11
No. of tri-iodide ions	1	1	1	1	1	2
No. of sodium ions	5	6	7	8	10	13
No. of acetonitrile molecules	112	139	173	219	276	351
No. of TiO_2 molecules	120	184	276	308	452	484

Table 3. Summary of the number of molecules of each species in the unit cells of the nanotube structure with different equivalent porosities

Nanotube structure	Equivalent porosity					
	0.60	0.65	0.70	0.75	0.80	0.85
Void volume ($Å^3$)	15169	18781	23597	30340	40452	57307
Total system volume ($Å^3$)	25282	28894	33710	40453	50565	67420
No. of iodide ions	5	6	7	9	12	17
No. of tri-iodide ions	1	1	1	1	1	2
No. of sodium ions	6	7	8	10	13	19
No. of acetonitrile molecules	147	185	237	307	413	580
No. of TiO_2 molecules	268	268	268	268	268	268

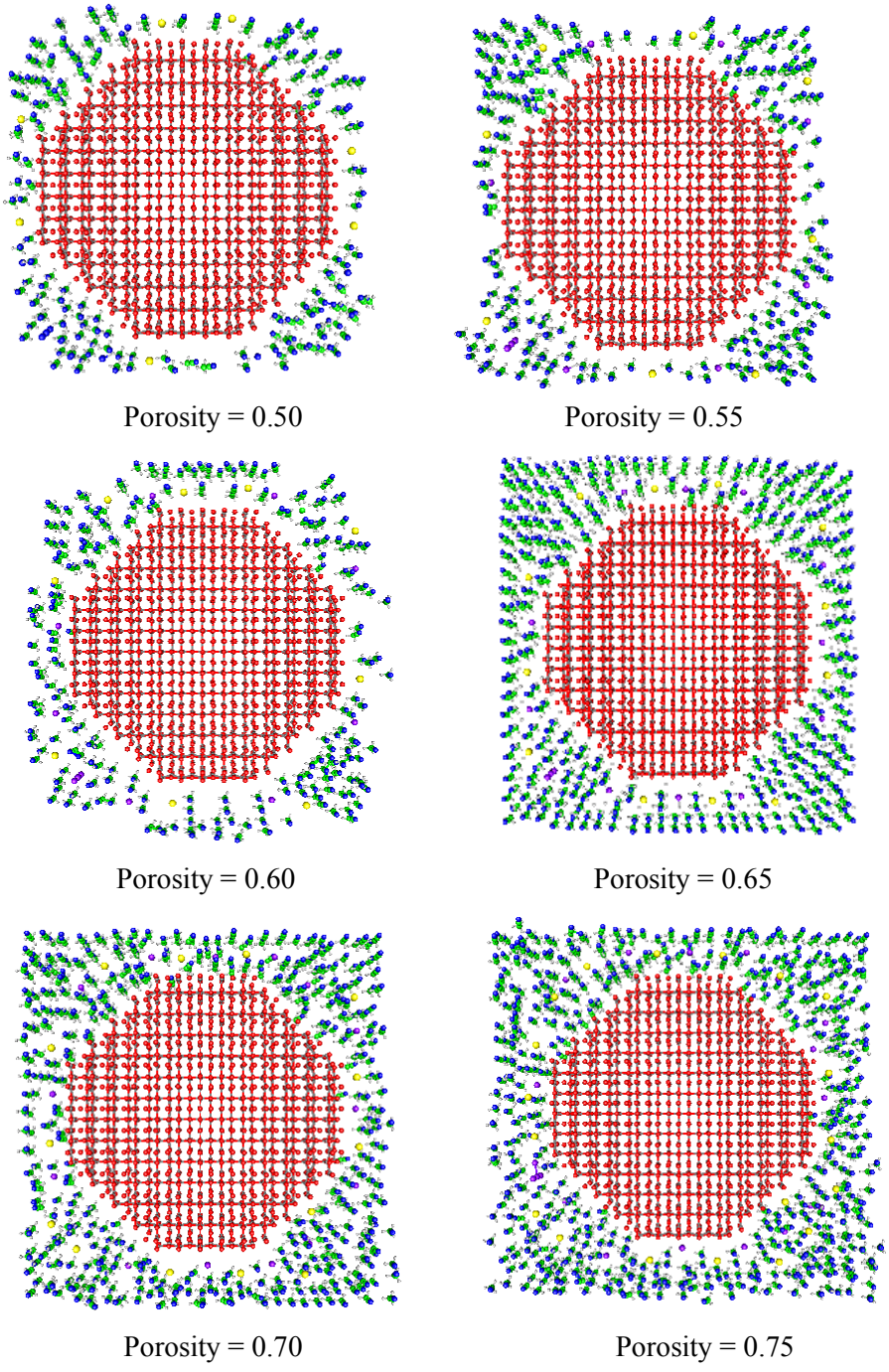

Figure 3: Unit cells and the initial distribution of the molecules among the nanorod array configuration (equivalent porosity=0.50˜0.75)

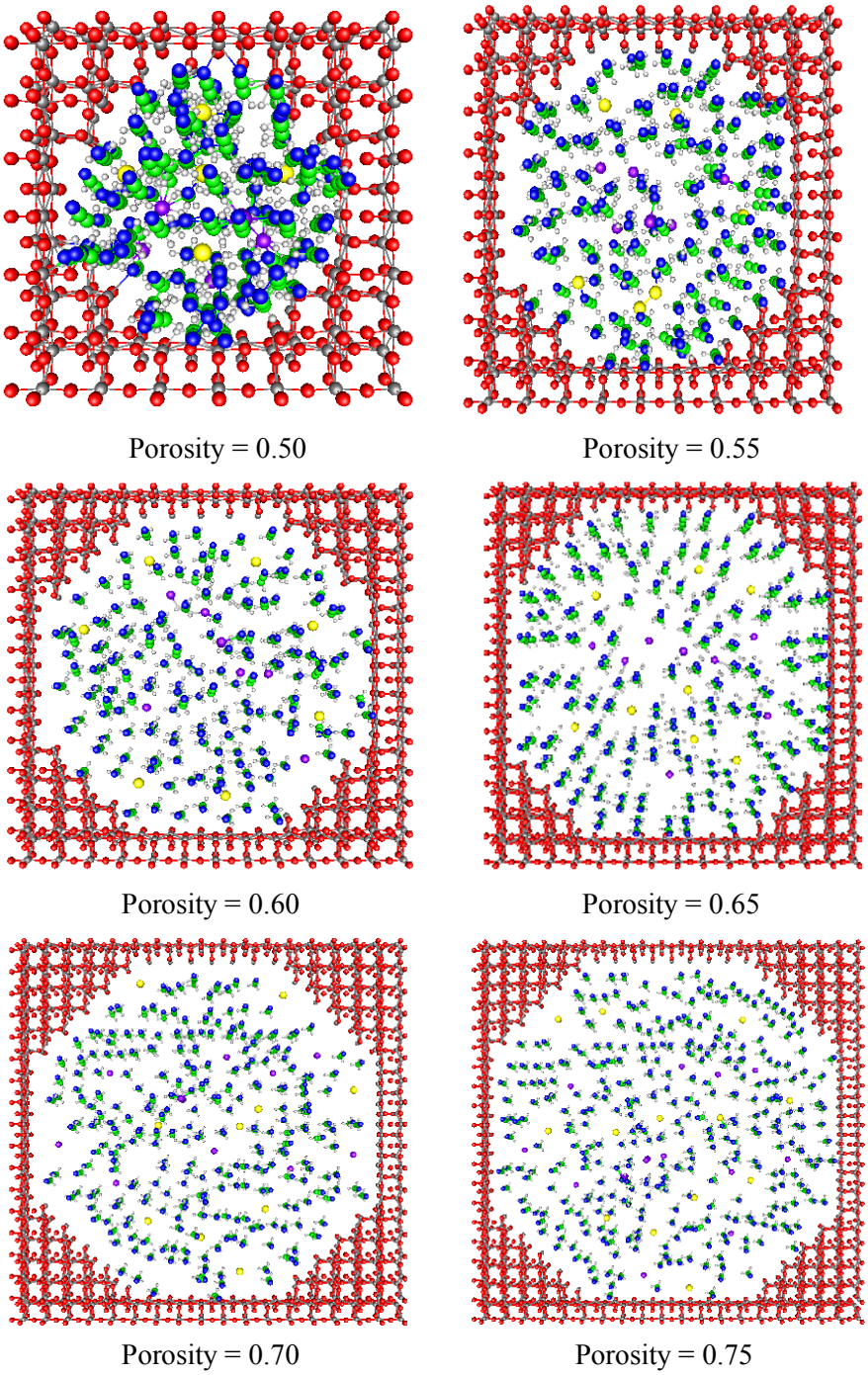

Figure 4: Unit cells and the initial distribution of the molecules among the nanowell array configuration (equivalent porosity=0.50˜0.75)

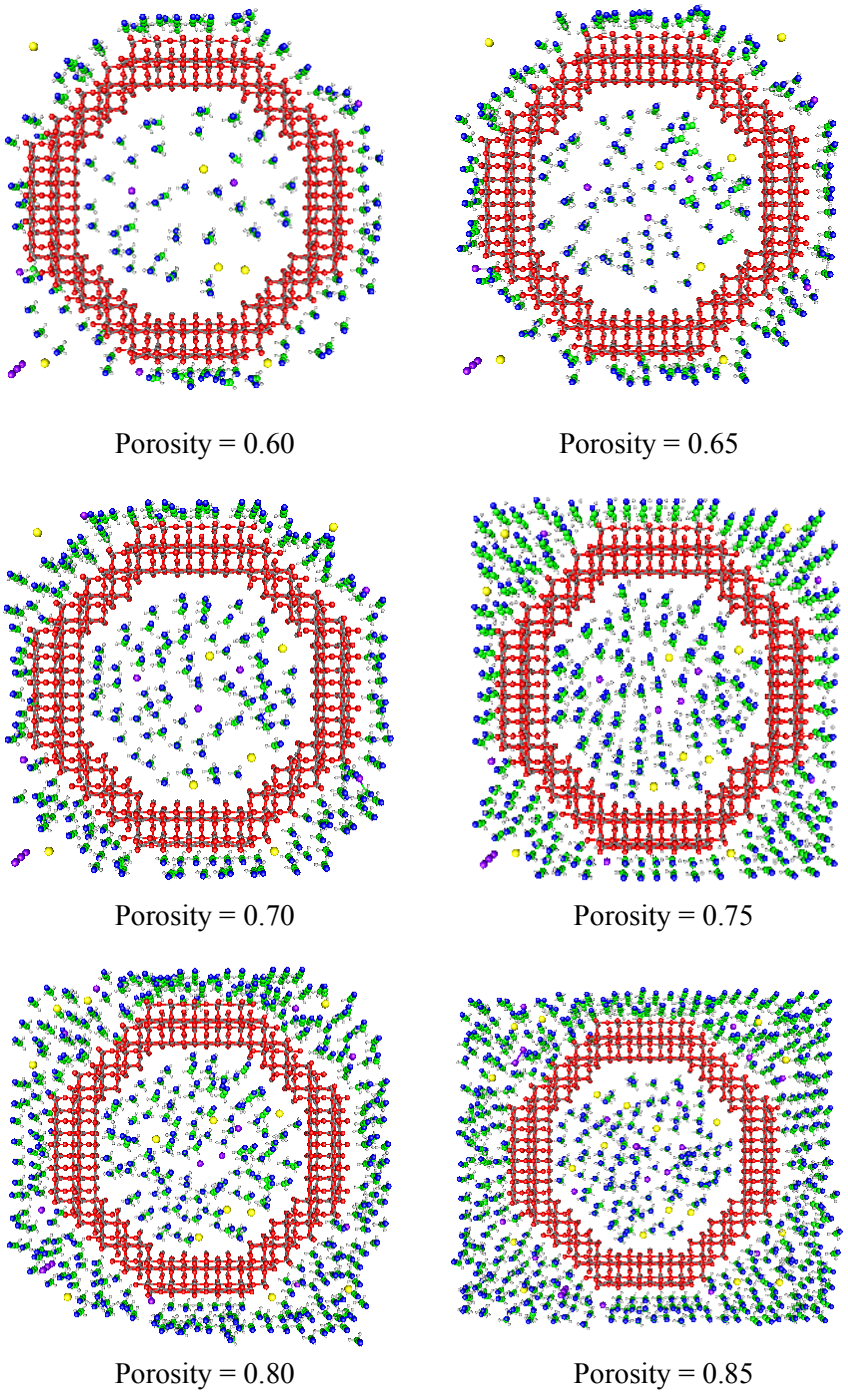

Figure 5: Unit cells and the initial distribution of the molecules among the nanotube array configuration (equivalent porosity=0.60˜0.85)

Molecular dynamics (MD) simulations were carried out on an IBM P690 workstation using the software DLPOLY [Smith, and Leslie (2006)]. A simulation with a period of 500ps at constant number of particles (N), constant volume (V) and constant temperature (T) was performed. The temperature was maintained at the desired value by the Berendsen thermostat algorithm with a relaxation time of 1.0 ps. Interactions separated more than 10Å were neglected and Newton's equations were integrated by the Verlet scheme with a time step of 1.0 fs. Three-dimensional periodic boundary conditions were applied and all the bond lengths were kept constant by the Shake algorithm. The periodic boundary conditions were used to simulate six equivalent porosities of nanorod, nanowell and nanotube arrays. The purpose is to predict the effective diffusion coefficients in the void volume among the nanoarrays.

4 Experimental

A rotating disk electrode (RDE) experiment was carried out to measure the free diffusion coefficients of both iodide and tri-iodide ions. The test apparatus, as shown in Figure 6, consists of a polished disc surrounded by an insulating sheath with a substantially larger diameter. The disk electrode is rotated about an axis perpendicular to the base of the device. The rotating disk acts as a pump, pulling the solution upward and then throwing it outward. According to the Nernst diffusion layer model, the flow pattern can be divided into two zones. The first zone, close to the electrode surface and with thickness δ, is assumed to have a totally stagnant layer where diffusion is the only mode of mass transport. The second zone is a strong convection region where all species concentrations are constant [Nikolic, Exposito, Iniesta, Gonzalez-Garcia, and Montiel (2000)]. Levich (1962) deduced a semi-empirical expression relating the thickness (δ) of the first zone with experimental parameters such as: the diffusion coefficient (D), the rotation speed of the electrode (ω) and the kinematic viscosity (ν) of the solvent. The expression is:

$$\delta = 1.61\nu^{0.166}D^{0.33}\omega^{-0.5} \tag{5}$$

The concept of the Nernst diffusion layer permits a trivial derivation of the current density at the RDE when the electrode reaction is mass-transport controlled. Since the surface concentration of the electro-active species is zero, the limiting current density (j_L) is given by:

$$j_L = nFDc\delta^{-1} \tag{6}$$

where n is the number of electrons involved in the electrode reaction; F is the Faraday constant; c is the concentration of the electro-active species in the bulk

solution with a value of 0.768 gcm^{-3}. Finally, combining equations (5) and (6) leads to the Levich equation:

$$j_L = 0.62nFD^{0.67}\nu^{-0.166}c\omega^{0.5} \tag{7}$$

Hence, the limiting current density is proportional to the concentration and the diffusion coefficient can be determined when the kinematic viscosity is given.

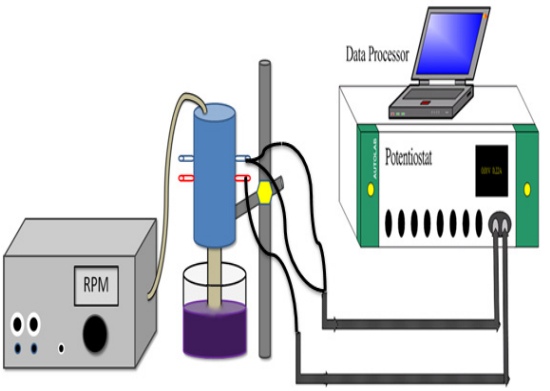

Figure 6: Schematic of the rotating disk electrode (RDE) apparatus

5 Mass Transfer and Photovoltaic Performance

To predict the solar cell performance, a computational mass transfer model was derived to describe the diffusion transport of the redox couple (I^-/I_3^-). Based on Fick's 2^{nd} law of diffusion under steady state, the ionic transport can be described by differential equations with respect to the distance (x) from the base plate of the nano-array:

$$D_{I_3^- na}\frac{d^2[I_3^-]_{na}(x)}{dx^2} + \frac{1}{2}(IPCE)\frac{d}{dx}P_i e^{-kx} = 0 \tag{8}$$

$$D_{I^- na}\frac{d^2[I^-]_{na}(x)}{dx^2} - \frac{3}{2}(IPCE)\frac{d}{dx}P_i e^{-kx} = 0 \tag{9}$$

$$\frac{d^2[I_3^-]_b(x)}{dx^2} = 0 \tag{10}$$

$$\frac{d^2[I^-]_b(x)}{dx^2} = 0 \tag{11}$$

where D_{I3^-na} is the effective diffusion coefficient of the tri-iodide in the nano-array, D_{I^-na} is the effective diffusion coefficient of the iodide ions, $[I_3^-]_b$ and $[I^-]_b$ are the tri-iodide and iodide concentrations in the bulk solution. *IPCE* represents the incident photon-to-current efficiency, P_i is the incident light intensity ($100 mW cm^{-2}$ at AM 1.5), and k is a photocurrent parameter which is a function of the dye molecules' extinction coefficient [Junghänel, and Tributsch (2005)]. In order to predict the photovoltaic performance, the calculation of the depletion rate of the redox charge at the boundary was needed. From Fick's 1^{st} law, the molar concentration flux at the boundary is expressed by:

$$N_j = D_{j_{eff}} \frac{\partial C_j}{\partial x} \qquad j = I^-, I_3^- \tag{12}$$

where $\frac{\partial C_j}{\partial x}$, at the right hand side, can be derived from the Butler-Volmer equation [Oldham, and Myland (1994)], which is written as:

$$\frac{\partial C_j}{\partial x} = \frac{A j_0 C_j}{nFD_{eff}C_{ref}^{\gamma}} \left[\exp\left(\frac{\alpha F}{RT}\eta\right) - \exp\left(-\frac{(1-\alpha)F}{RT}\eta\right) \right] \tag{13}$$

In the above equation, A is the reaction area, j_0 is the exchange current density, n is the number of electrons involved in the reaction, F is the Faraday constant, C_{ref} is the reference species concentration, α is the transfer coefficient for the reaction, R is the gas constant, T is the operation temperature, γ is the reaction order and η is the over-potential. The local current density at the electrode surface can be evaluated by $i = nFN_j$, and the power density of the solar cell at a precribed voltage, V_{sc}, is calculated by $P_{sc} = iV_{sc}$.

6 Simulation Results and Discussion

6.1 System Equilibration

In the NVT simulation, the time for reaching equilibration was set to be 50 ps and the following 450 ps were run for a statistical analysis. Figure 7 and Figure 8 show that the nanorod array design's total potential energy and system temperature, respectively, versus elapsed time converged in all the simulation cases. Fluctuations in the total potential energy and temperature of the system were less than ± 5 % for all the nanostructures. The statistical evaluation that followed is described in the next section.

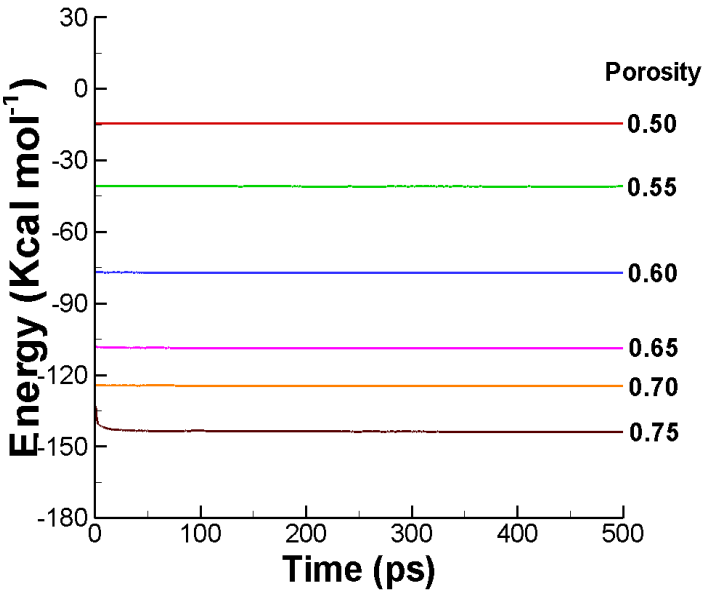

Figure 7: Potential energy variation versus elapsed time during molecular simulation at different porosities of 0.50, 0.55, 0.60, 0.65, 0.70 and 0.75 respectively for nanorod cases

6.2 Diffusion Coefficient Analysis

A statistical method to analyze the predicted mobility of iodide/tri-iodide ions, whose result will be entered in the Einstein relation for evaluating the diffusion coefficient, is described. The mobility of the iodide/tri-iodide ions can be analyzed using the mean square displacement (MSD) versus time diagram. The MSD is defined statistically by:

$$MSD = \frac{1}{N}\sum_{n=1}^{N}\left\langle [\vec{r}_n(t_o+t) - \vec{r}_n(t_o)]^2 \right\rangle \tag{14}$$

where N is the total number of molecules in the simulation system; $\vec{r}_n(t)$ is the position vector of atom n at time t; t_0 is the initial time step; and the triangular brackets, $< >$, represent the time average algorithm. The MSD curves tend to be linear, which infer these ions are diffusing continuously in the system during the simulation. Figure 9 shows that the iodide ions have a greater slope in the MSD curve that can be attributed to their molecular weight which is smaller than the tri-

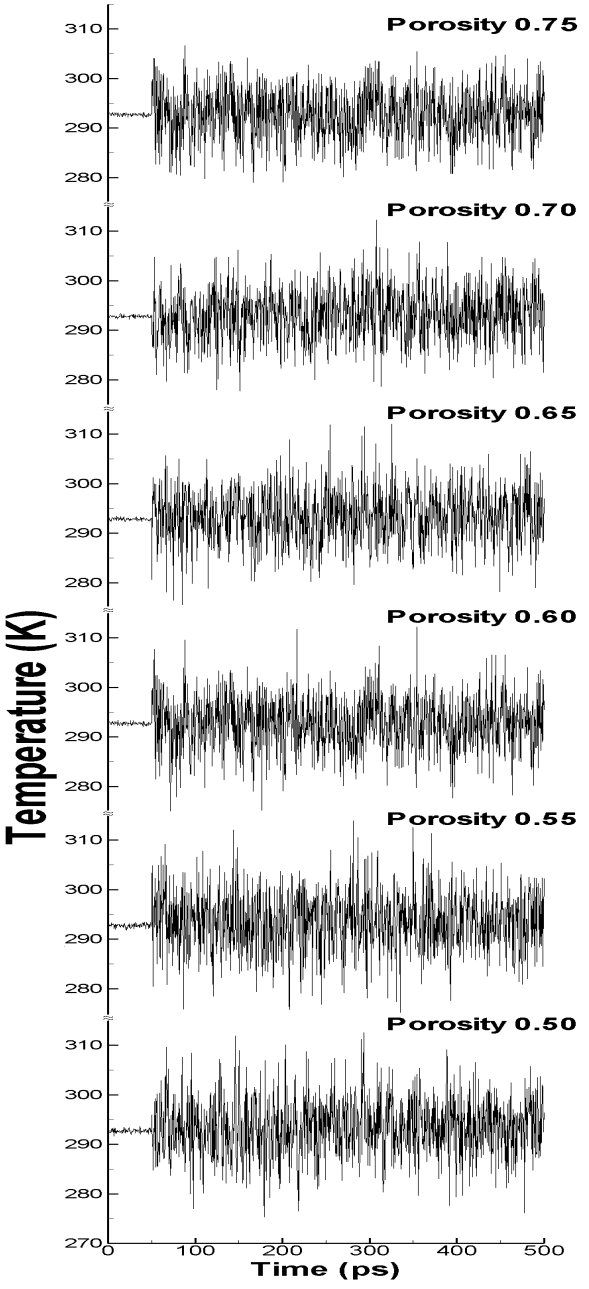

Figure 8: System temperature variation versus elapsed time during molecular simulation at different porosities of 0.50, 0.55, 0.60, 0.65, 0.70 and 0.75 respectively for nanorod cases

iodide. This was done for all three nano structures and at different porosities, but only the nanorod structure's result at a porosity of 0.65 is shown. It is observed that the MSD curves are almost linearly proportional to the elapsed time.

With these results, it is now possible to evaluate the diffusion coefficient using the Einstein relation stated below:

$$D = \frac{1}{6N} \lim_{t \to \infty} \frac{d}{dt} \sum_{n=1}^{N} \left\langle [\vec{r}_n(t_o + t) - \vec{r}_n(t_o)]^2 \right\rangle \tag{15}$$

where D is the diffusion coefficient, N is the total number of molecules in the simulation system and $\vec{r}_n(t)$ is the position vector of atom n at time t.

The predicted free diffusion coefficients of the iodide and tri-iodide ions are compared with the experimental data and are shown in Figure 10. The comparison shows a very good agreement between simulation and experimental results and the error lies within 2%. For iodides, the predicted free diffusion coefficient is $1.30 \times 10^{-9} m^2 s^{-1}$and the experimental result is$1.28 \times 10^{-9} m^2 s^{-1}$. For tri-iodides, it is $1.08 \times 10^{-9} m^2 s^{-1}$for prediction and $1.06 \times 10^{-9} m^2 s^{-1}$for experiment. Note that an increasing porosity (void volume divided by system volume) may increase the diffusion coefficient but decrease the reaction area, as shown in Figure 10. The reaction area ratio is around 12,415 times the original surface (with a porosity equal to unity) when the porosity is equivalent to 0.5 in the nanorod array design, as shown in the right hand side of Figure 10.

The trend of the predicted diffusion coefficients at different porosities in the nanorod array design shows proportionality to the equivalent porosity. This can be explained by a decreasing influence from the TiO_2 due to a greater proportion of the void volume which promotes the mobility of ions in the confined space. Figure 11 shows a trend of the predicted diffusion coefficients versus the equivalent porosity of the nanowell array design. This trend is very similar to that shown by the nanorod array design.

However, the diffusion coefficients for nanowell design are slightly lower than those for the nanorod at the same porosity. The reaction area can increase to 21,667 times the original area (porosity = 1) when the porosity is equivalent to 0.5.

The third array design is the nanotube type, constructed by combining both nanorod and nanowell structures. Figure 12 shows that the nanotube array has the lowest diffusion coefficients and the highest reaction area ratio (30,063) when the porosity is equivalent to 0.6, compared to the previous two designs. It is important to note that, in all designs, the diffusion coefficients of iodide and tri-iodide ions show no significant increase at a higher porosity. An optimal porosity that maximizes both reaction area and diffusion coefficient can be evaluated. To find this optimized

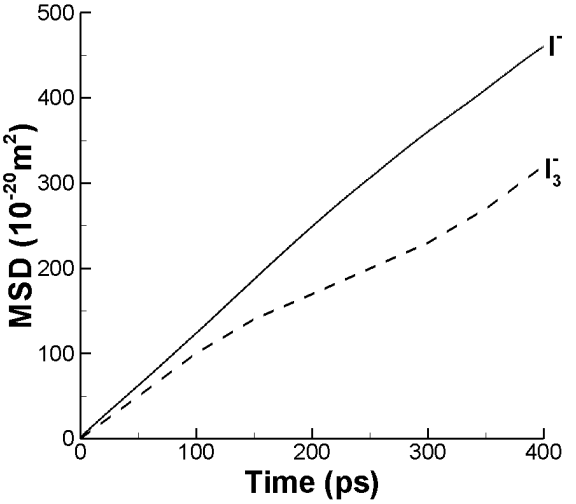

Figure 9: Mean square displacement (MSD) of iodide and tri-iodide ions at 0.5M I^- + 0.055M I_3^- in nanorod case with porosity at 0.65

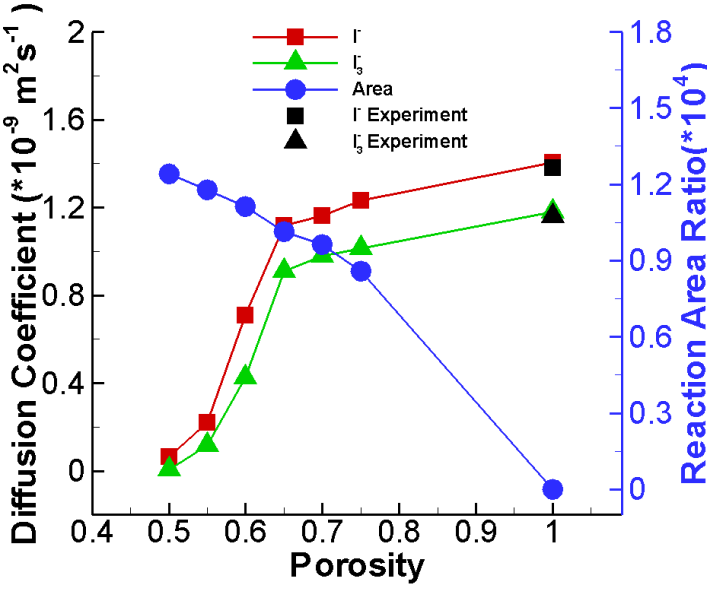

Figure 10: Comparison between predicted and experimental diffusion coefficients of iodide and tri-iodide ions and reaction area ratio versus different porosities of 0.50, 0.55, 0.60, 0.65, 0.70, 0.75 and 1.0 respectively for nanorod array

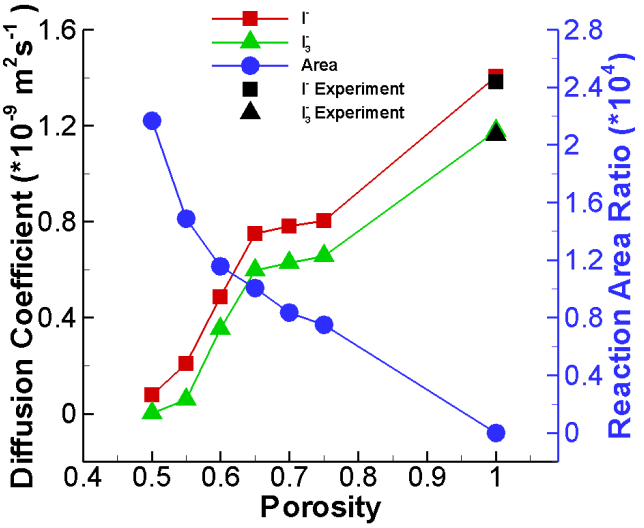

Figure 11: Comparison between predicted and experimental diffusion coefficients of iodide and tri-iodide ions and reaction area ratio versus different porosities of 0.50, 0.55, 0.60, 0.65, 0.70, 0.75 and 1.0 respectively for nanowell array

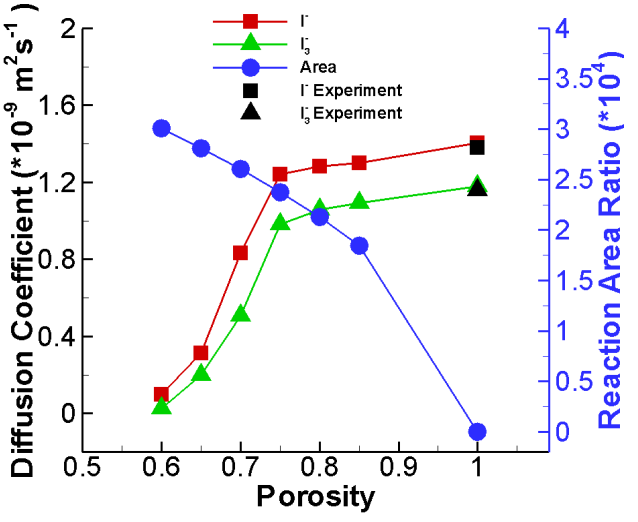

Figure 12: Comparison between predicted and experimental diffusion coefficients of iodide and tri-iodide ions and reaction area ratio versus different porosities of 0.60, 0.65, 0.70, 0.75, 0.80, 0.85 and 1.0 respectively for nanotube array

porosity, one plots the product of the diffusion coefficient ratio (the diffusion coefficient at each porosity divided by the free diffusion coefficient) multiplied by the reaction area ratio (the reaction area at each porosity divided by the original reaction area at porosity one).

Figure 13 shows that the optimized porosity for both the nanorod and nanowell design is 0.65. The nanotube array design has the highest value of the product of the diffusion coefficient ratio times the reaction area ratio (2.09 for I^- and 1.98 for $I_3{}^-$) at the optimized porosity close to 0.75.

6.3 Solar Cell Performance Prediction

By inputting an averaged IPCE value from an experimental IPCE spectrum diagram (shown as an inset in Figure 14(a)) in the simulation, the I-V performance can be predicted for the novel nanorod/nanowell/nanotube solar cells. The baseline is the measured performance of a nano-crystalline film dye-sensitized solar cell, fabricated in our laboratory, using N719 dyes. Figure 14 shows that the maximum current density is 20.1 $mAcm^{-2}$ for the nanotube array design and that corresponds to the maximum power density of 10.1 $mWcm^{-2}$. Compared to the baseline nanofilm design at 13.1 $mAcm^{-2}$and 6.1 $mWcm^{-2}$, the current density can be improved by 53% and power density by 66%. The performance improvement can be attributed to a higher reaction area and diffusion coefficient product exhibited by the nanotube when compared to the nanorod and nanowell structures at their respective optimized porosities.

7 Conclusions

This paper has investigated the ionic diffusion of the electrochemical active species ($I^-/I_3{}^-$) on the porous electrode surface for photo-electrochemical solar cells. The electrode was modeled using three different nano-structures: nanorod, nanowell and nanotube arrays. This computer simulation approach, instead of a purely experimental one, was conducted because of the difficulty in measuring the effective diffusion coefficient in such a small and confined environment. Still, an experimental approach was used to validate the accuracy of the molecular simulation at a free diffusion of the redox ions by using a rotating disk electrode experiment. The effective diffusion coefficient in the porous nano-arrays bears a strong relationship to the equivalent porosity. MSD diagrams show that the iodide/tri-iodide ions all behave as nanofluids due to the linearly increasing trend between the MSD curve and the elapsed time. Three-dimensional periodic boundary conditions were set up to simulate the design of the nano-arrays, which include: nanorod, nanowell and nanotube configurations in this paper. Simulation results reveal that the nanotube array design has the greatest value (2.09 for I^- and 1.98 for $I_3{}^-$) of the product for

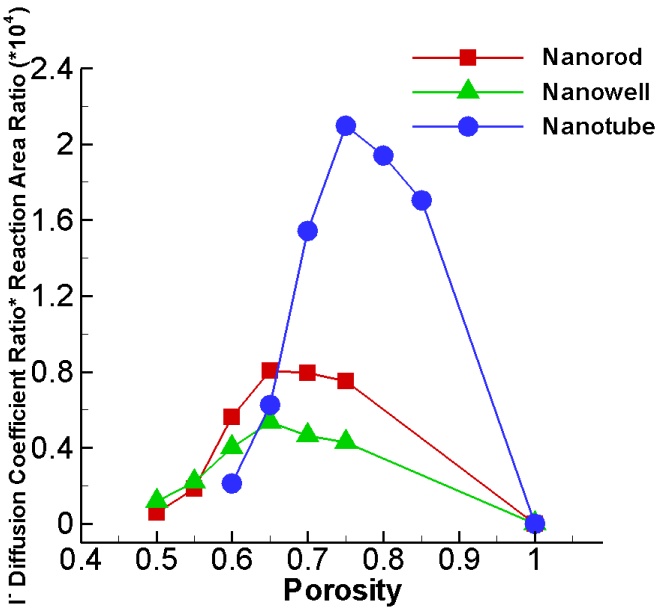

(a)

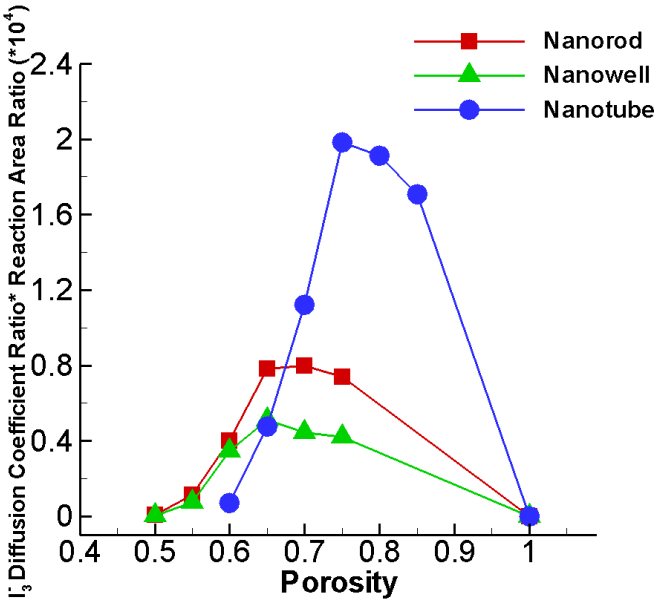

(b)

Figure 13: Comparison of diffusion coefficient ratio times reaction area ration versus porosity in nanorod, nanowell and nanotube designs for (a) iodide and (b) triiodide ions. The result indicates that the nanotube array at porosity 0.75 has the optimized value.

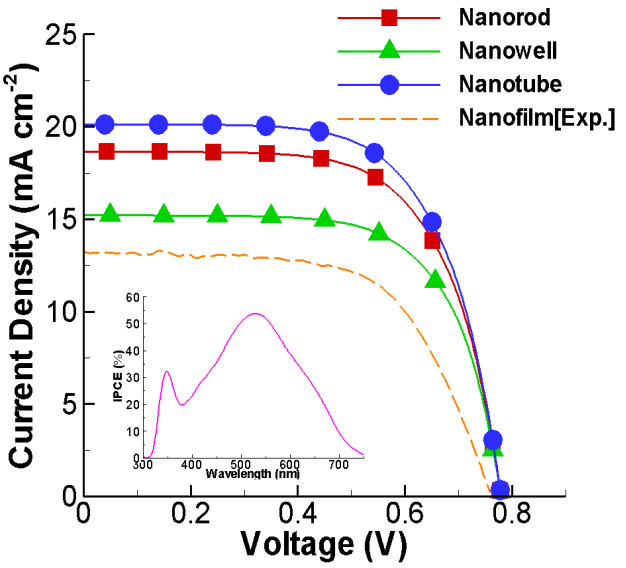

(a)

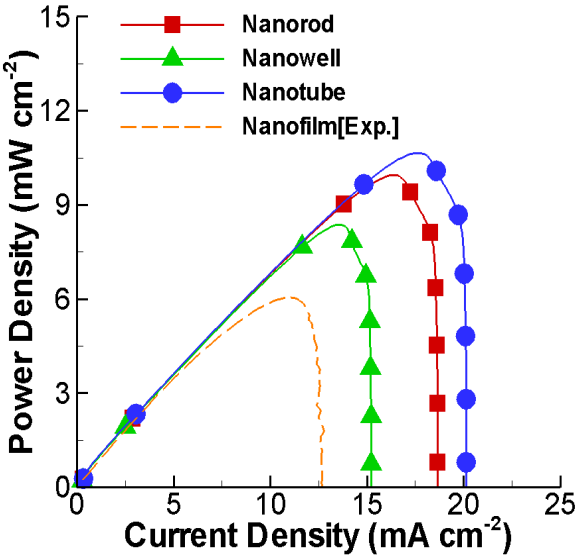

(b)

Figure 14: Predicted photovoltaic performance in nanorod/nanowell/nanotube designs, and compared to the measured performance of a nano-crystalline film DSSC (using N719 dyes). The inset shows the IPCE spectrum obtained from an experiment, which is averaged and input to the mass transfer model. The simulation results show that (a) there is a 53% improvement in the current density, and (b) a 66% improvement in the power density diagrams.

the diffusion coefficient ratio times the reaction area ratio at an equivalent porosity of 0.75. With this optimized porosity, the photovoltaic current density and power density can be increased by 53% and 66%, respectively. In the near future, modern nanotechnologies can further improve this performance of photo-electrochemical solar cells even further. The molecular simulation tool developed in this paper will play an important role in future designs to screen those novel ideas.

Acknowledgement: Thanks are due to the National Science Council of Taiwan and National Tsing Hua University Boost Program who supported this research under the grant numbers: NSC 98-2221-E-007-108-MY3 and NTHU 99N2521E1. We are also grateful to the National Center for High-Performance Computing for the generous computer time and facilities.

References

Allen, M. P.; Tildesley, D. J. (1987): *Computer Simulation of Liquids.* Oxford University Press.

Chen, C.C.; Jehng, W.D.; Li, L.L.; Diau, W.G. (2009): Enhanced efficiency of dye-sensitized solar cells using anodic titanium oxide nanotube arrays. *J. Electrochem. Soc.,* vol. 156, pp. C304–C312.

Chen, C.Y.; Wang, M.; Li, J.Y.; Pootrakulchote, N.; Alibabaei, L.; Ngoc-Le, C.H.; Decoppet, J.D.; Tsai, J.H.; Grätzel, C.; Wu, C.G.; Zakeeruddin, S.M.; Grätzel, M. (2009): Highly efficient light-harvesting ruthenium sensitizer for thin-film dye-sensitized solar cells. *J. Am. Chem. Soc.,* vol. 3, pp. pp.3103–3109.

Chen, P.Y.; Chiu, C.P.; Hong, C.W. (2009): Molecular structure and transport dynamics in Nafion and sulfonated poly (ether ether ketone ketone) membranes. *J. Power Sources,* vol. 194, pp. 746–752.

Chen, W.H.; Miranda, A.G.; Hong, C.W. (2011): Parametric studies on the photovoltaic performance improvement of a novel nanotube photo-electrochemical solar cell. *J. Electrochem. Soc.*, vol. 158 (5), pp. 57-64.

Chen, Y.H.; Chen, W.H.; Hong, C.W. (2009): Molecular simulation and performance prediction of photoelectrochemical solar cell. *J. Electrochem. Soc.,* vol. 156 (11), pp. 163–168.

Deb, S.K. (2005): Dye-sensitized TiO_2 thin-film solar cell research at the National Renewable Energy Laboratory (NREL). *Sol. Energy Mater. Sol. Cell,* vol. 88, pp.1–10.

Gong, D.; Grimes, C.A.; Varghese, O.K.; Hu, W.; Singh, R.S.; Chen, Z.; Dickey, E.C. (2001): Titanium oxide nanotube arrays prepared by anodic oxida-

tion. *J. Mater. Res.,* vol. 16, pp. 3331–3334.

Grätzel, M. (2009): Recent advances in sensitized mesoscopic solar cells. *Accounts of Chemical Research,* vol. 22, pp. 1788–1798.

Green, M.A.; Emery, K.; Hisikawa, Y.; Warta, W. (2009): Solar cell efficiency tables (version 34). *Prog, Photovoltaics: Res. Appl.,* vol. 17, pp. 320–326.

Hypercube Inc., (2002): *HyperChem reference manual.* Chapter 8.

Ide, K.; Fujimoto, M.; Kado, T.; Hayase, S. (2008): Increase in intensity of electrochemiluminescence from cell consisting of TiO_2 nanohole array film. *J. Electrochem. Soc.,* vol. 155, pp. B645–B649.

Jiu, J.; Isoda, S.; Wang, F.; Adachi, M. (2006): Dye-sensitized solar cells based on a single-crystalline TiO_2 nanorod-film. *J. Phys. Chem. B,* vol. 110, pp. 2087–2092.

Junghänel, M.; Tributsch, H. (2005): Role of nanochemical environments in porous TiO_2 in photocurrent efficiency and degradation in dye-sensitized solar cells. *J. Phys. Chem. B,* vol. 109, pp. 22876–22883.

Kang, S.H.; Choi, S.H.; Kang, M.S.; Kim, J.Y.; Kim, H.S.; Hyeon, T.; Sung, Y.E. (2008): Nanorod-based dye-sensitized solar cells with improved charge collection efficiency. *Adv. Mater.,* vol. 20, pp. 54–58.

Kim, D.; Ghicov, A.; Albu, S.P.; Schmuki, P. (2008): Bamboo-type TiO_2 nanotubes: improved conversion efficiency in dye-sensitized solar cells. *J. Am. Chem. Soc.,* vol. 130, pp. 16454–16455.

Kislyuk, V.V.; Dimitriev, O.P. (2008): Nanorods and nanotubes for solar cells. *J. Nanosci. Nanotechnol.,* vol. 8, pp. 131–148.

Lee, B.H.; Song, M.Y.; Jang, S.Y.; Jo, S.M.; Kwak, S.Y.; Kim, D.Y. (2009): Charge transport characteristics of high efficiency dye-sensitized solar cells based on electrospun TiO_2 nanorod photoelectrodes. *J. Phys. Chem. C,* vol.113, pp. 21453–21457.

Lee, S.F.; Hong, C.W. (2009): Computer modeling of ionic conductivity in low temperature doped ceria solid electrolytes. *CMC: Computer, Materials, & Continua,* vol. 12(3), pp. 223–235.

Levich, V.G. (1962): *Physicochemical Hydrodynamics.* Prentice-Hall.

Li, D.; Saheli, G.; Khaleel, M.; Garmestani, H. (2006): Microstructure optimization in the fuel cell electrodes using materials design. *CMC: Computer, Materials, & Continua,* vol. 4, pp. 31–42.

Marco, L.D.; Manca, M.; Giannuzzi, R.; Malara, F.; Melcarne, G.; Ciccarella, G.; Zama, I.; Cingolani, R.; Gigli, G. (2010): Novel preparation method of TiO_2-

nanorod-based photoelectrodes for dye-sensitized solar cells with improved light-harvesting efficiency. *J. Phys. Chem. C,* vol. 114, pp. 4228–4236.

Mayo, S.L.; Olfason, B.D.; Goddard, W.A. (1990): Dreiding: A general force field for molecular simulations. *J. Phys. Chem.,* vol. 94, pp. 8897–8909.

Nikolic, J.; Exposito, E.; Iniesta, J.; Gonzalez-Garcia, J.; Montiel, V. (2000): Theoretical concepts and applications of a rotating disk electrode. *J. Chem. Educ.,* vol. 77, pp. 1191–1194.

Oldham, K. B.; Myland, J.C. (1994): *Fundamentals of Electrochemical Science.* Academic.

Paula, U.E.; Colavita, E.; Doescher, M.S.; Schiza, M.; Myrick, M.L. (2002): Construction and characterization of a nanowell electrode. *Nano Lett.,* vol. 2, pp. 641–645.

Roy, P.; Kim, D.; Lee, K.; Spiecker, E.; Schmuki, P. (2010): TiO_2 nanotubes and their application in dye-sensitiazed solar cells. *Nanoscale,* vol. 2, pp. 45–49.

Smith, W.; Leslie, M.; Forester, T. R. (2006): *The DL _POLY_2 user manual.* CCLRC, Daresbury Laboratory.

Tao, R. H.; Wu, J.M.; Xue, H. X.; Song, X. M.; Pan, X.; Fang, X. Q.; Fang, X. D.; Dai, S. Y. (2010): A novel approach to titania nanowire arrays as photoanodes of back-illuminated dye-sensitized solar cells. *J. Power Sources,* vol. 195, pp. 2989–2995.

Xu,C.; Shin, P.H.; Cao, L.; Wu, J.; Gai, D. (2010): Order TiO_2 nanotube arrays on transparent conductive oxide for dye-sensitized solar cells. *Chem. Mater.,* vol. 22, pp. 143–148.